INTERNATIONAL JOURNAL FOR NUMERICAL METHODS IN FLUIDS
Int. J. Numer. Meth. Fluids 2009; **61**:237–254
Published online 6 November 2008 in Wiley InterScience (www.interscience.wiley.com). DOI: 10.1002/fld.1948

Some results on the accuracy of an edge-based finite volume formulation for the solution of elliptic problems in non-homogeneous and non-isotropic media

Darlan Karlo Elisiário de Carvalho*,†, Ramiro Brito Willmersdorf and Paulo Roberto Maciel Lyra

Departamento de Engenharia Mecânica (DEMEC), Universidade Federal de Pernambuco (UFPE), Av. Acadêmico Hélio Ramos S/N, CEP: 50740-530, Recife-PE, Brazil

SUMMARY

The numerical simulation of elliptic type problems in strongly heterogeneous and anisotropic media represents a great challenge from mathematical and numerical point of views. The simulation of flows in non-homogeneous and non-isotropic porous media with full tensor diffusion coefficients, which is a common situation associated with the miscible displacement of contaminants in aquifers and the immiscible and incompressible two-phase flow of oil and water in petroleum reservoirs, involves the numerical solution of an elliptic type equation in which the diffusion coefficient can be discontinuous, varying orders of magnitude within short distances. In the present work, we present a vertex-centered edge-based finite volume method (EBFV) with median dual control volumes built over a primal mesh. This formulation is capable of handling the heterogeneous and anisotropic media using structured or unstructured, triangular or quadrilateral meshes. In the EBFV method, the discretization of the diffusion term is performed using a node-centered discretization implemented in two loops over the edges of the primary mesh. This formulation guarantees local conservation for problems with discontinuous coefficients, keeping second-order accuracy for smooth solutions on general triangular and orthogonal quadrilateral meshes. In order to show the convergence behavior of the proposed EBFV procedure, we solve three benchmark problems including full tensor, material heterogeneity and distributed source terms. For these three examples, numerical results compare favorably with others found in literature. A fourth problem, with highly non-smooth solution, has been included showing that the EBFV needs further improvement to formally guarantee monotonic solutions in such cases. Copyright © 2008 John Wiley & Sons, Ltd.

Received 24 January 2008; Revised 11 July 2008; Accepted 10 September 2008

KEY WORDS: edge-based data structure; unstructured meshes; finite volume; elliptic equation; accuracy; heterogeneous and anisotropic media

*Correspondence to: Darlan Karlo Elisiário de Carvalho, Departamento de Engenharia Mecânica (DEMEC), Universidade Federal de Pernambuco (UFPE), Av. Acadêmico Hélio Ramos S/N, CEP: 50740-530, Recife-PE, Brazil.
†E-mail: dkarlo@uol.com.br, darlan@demec.ufpe.br

Contract/grant sponsor: Conselho Nacional de Desenvolvimento Científico e Tecnológico (CNPq)
Contract/grant sponsor: Agência Nacional do Petróleo (ANP-MCT)
Contract/grant sponsor: Fundação de Amparo à Ciência e Tecnologia do Estado de Pernambuco (FACEPE)

Copyright © 2008 John Wiley & Sons, Ltd.

1. INTRODUCTION

The task of modeling and simulating diffusion type problems in heterogeneous and anisotropic media can be a great challenge from a mathematical and numerical point of view. Abrupt variations in the permeability field (i.e. the diffusion coefficient) are common when modeling and simulating fluid flow in petroleum reservoirs and aquifers. Over the last decades, much effort has been spent in numerical methods that make use of unstructured meshes, such as the finite element method (FEM) and the finite volume method (FVM), due the fact that these methods allow for a better modeling of complex geometrical features and because they can easily incorporate mesh adaptive procedures. When handling conservation laws, FVM is particularly attractive as it conserves mass, globally and locally. It is well known that traditional two-dimensional 'five point' finite difference methods are unable to handle full tensors or non-orthogonal meshes. Besides, it can be proved that these schemes introduce first-order errors in the approximation of flux terms between discontinuous materials [1], making these methods unsuitable for the modeling and simulation of diffusion type problems in highly heterogeneous and anisotropic media.

Locally conservative schemes, such as the mixed finite element method (MFEM) and flux continuous finite volumes (FCFV), also called multipoint flux approximations (MPFA), have been extensively studied in literature [1–5]. In the context of flux flow in porous media, the recently developed FCFV are defined by assuming continuous pressures (pointwise or full continuity) and normal fluxes across control volumes (CV) interfaces [1, 3–5]. Despite of the high computational costs associated with these methods, particularly the MFEM, both methods are capable of handling full tensor elliptic equations in highly heterogeneous media using structured or unstructured meshes. It is worth remembering that the FEM, which is globally but not locally conservative (i.e. at the element level), requires some kind of flux recovery in order to formally guarantee local conservation [6].

In the present paper, we describe a node-centered finite volume formulation in which median dual CV (Donald's dual) are used with an edge-based data structure [7–12] in such a way that the geometrical coefficients are associated with the edges and nodes of the primal mesh. This formulation, which is capable of handling structured or unstructured meshes, and non-homogeneous and anisotropic media, has been chosen due to the fact that vertex-centered finite volume schemes are usually superior to the cell-centered schemes in terms of memory usage [7, 10], and because edge-based data structures are known to be computationally more efficient than their element-based counterparts [7] and also because they allow for the introduction of one dimensional like upwinding [13] when models incorporating advective transport are devised, such as in two-phase flows in porous media [11, 12]. In the present paper we have concentrated on the study of the accuracy and the convergence behavior of an edge-based finite volume scheme for the solution of elliptic equations with full tensor discontinuous coefficients, comparing it with other well-established formulations through the solution of some benchmark problems.

2. MATHEMATICAL FORMULATION

In the two-dimensional model, the equation that defines an elliptic problem in a heterogeneous and anisotropic medium can be written as

$$\nabla \cdot (-\underset{\sim}{K}(\mathbf{x})\nabla u) = f(\mathbf{x}) \quad \text{with } \mathbf{x} = (x, y) \in \Omega \subset \Re^2 \tag{1}$$

Copyright © 2008 John Wiley & Sons, Ltd.

DOI: 10.1002/fld

where

$$\underset{\sim}{K}(\mathbf{x}) = \underset{\sim}{K} = \begin{pmatrix} K_{xx} & K_{xy} \\ K_{yx} & K_{yy} \end{pmatrix} \tag{2}$$

is a symmetric matrix that is allowed to be discontinuous through the internal boundaries of the domain Ω.

In order to formally define an elliptic problem [14], we further assume that

$$K_{xx} K_{yy} \geqslant K_{xy}^2 \tag{3}$$

Integrating Equation (1) and applying the divergence theorem to its left side, yields

$$\int_{\Gamma} (-\underset{\sim}{K} \nabla u) \cdot \mathbf{n} \partial\Gamma = \int_{\Omega} f \partial\Omega \tag{4}$$

Equation (4), which is the integral form of Equation (1), defines, for instance, the pressure field for the fluid flow of oil and water in heterogeneous and anisotropic petroleum reservoirs or for the transport of contaminants in aquifers [10–12].

3. NUMERICAL FORMULATION

As previously mentioned, in the present work, we have adopted a node-centered finite volume procedure with median dual CV built over a triangular primary mesh, in which the coefficients necessary to our calculation are associated with the edges and to the nodes of the primary mesh [7, 8, 10–12, 15]. These edge and node coefficients are pre-computed in a pre-processing stage from the more traditional element data structure, which are commonly used in the FEM context.

For a general node I of the mesh, using the EBFV, Equation (4) can be approximated as

$$\sum_{L_I \in \Omega} \mathbf{F}_{IJ_L}^{\Omega} \cdot \mathbf{C}_{IJ_L} + \sum_{L_I \in \Gamma} \mathbf{F}_{IJ_L}^{\Gamma} \cdot \mathbf{D}_{IJ_L} = f_I V_I \tag{5}$$

where $\mathbf{F}_{IJ_L} = -\underset{\sim}{K} \nabla u_{IJ_L}$ is the flux function defined at the control surface, V_I is the volume of the CV surrounding node I, the upper index Ω represents approximations that are associated with every edge IJ_L of the primary mesh, which is connected to node I, Γ refers only to boundary edges connected to that node, the summation $\sum_{L_I \in \Omega}$ is performed over the internal edges connected to node I and $\sum_{L_I \in \Gamma}$ is only performed over boundary edges. The geometrical coefficients $\mathbf{C}_{IJ_L}$ and $\mathbf{D}_{IJ_L}$ are defined as

$$\begin{aligned} \mathbf{C}_{IJ_L} &= A_{K+1} \mathbf{n}_{K+1} + A_K \mathbf{n}_K \\ \mathbf{D}_{IJ_L} &= A_L \mathbf{n}_L \end{aligned} \tag{6}$$

In Equation (6), A_K, A_{K+1} and A_L are the areas of the control surfaces associated with the control surface normals $\mathbf{n}_K$, $\mathbf{n}_{K+1}$ and $\mathbf{n}_L$. Further details can be found in [9, 11].

In order to approximate the mid-edge gradients/fluxes required in Equation (5), different strategies can be devised [16]. The classical edge-based approach involves using a simple two-point flux approximation (TPFA), in which mid-edge fluxes are formally second-order accurate only if the media is isotropic and the straight lines that connects two adjacent nodes and the control surfaces

Copyright © 2008 John Wiley & Sons, Ltd.

DOI: 10.1002/fld

are orthogonal to each other, as in the case of the Voronoi tessellations [4] and structured quadrilateral meshes. Schemes using such approaches are equivalent to the so-called control volume finite difference methods.

In the present paper, we use a different approach that has been originally devised by Crumpton *et al.* [8] for the discretization of diffusion terms in the Navier–Stokes equations. In this approach, in order to obtain the final discrete system of equations, we first compute nodal gradients as functions of the discrete scalar field, and then we use these gradients to compute the elliptic terms in a second step [8–12, 15]. The gradients computed in the first step in a finite volume fashion are used to calculate the cross diffusion terms, which naturally arise when we are handling full tensor problems (i.e. $K_{xy}=K_{yx}\neq 0.0$) or when we are using non-orthogonal meshes, as both problems can be seen as equivalent [1].

In order to compute the nodal gradient, we make use of the divergence theorem to integrate the gradient of the scalar variable at node I, obtaining

$$\int_{\Omega_I} \nabla u_I \partial\Omega_I = \int_{\Gamma_I} u_I \mathbf{n} \partial\Gamma \tag{7}$$

Assuming that the average gradient $\overline{\nabla} u_I$ in the CV can be defined as

$$\overline{\nabla} u_I = \left(\int_{\Omega_I} \nabla u_I \partial\Omega_I \right) \Big/ V_I \tag{8}$$

Similarly to Equation (5), and by dropping out the over bar, we can write the discrete form of Equation (7) as

$$\nabla u_I V_I = \left(\sum_{L_I \in \Omega} u^{\Omega}_{IJ_L} \mathbf{C}_{IJ_L} + \sum_{L_I \in \Gamma} u^{\Gamma}_{IJ_L} \mathbf{D}_{IJ_L} \right) \tag{9}$$

Additionally, we adopt the following linear edge approximations:

$$u^{\Omega}_{IJ_L} = \frac{u_I + u_{J_L}}{2} \quad \text{and} \quad u^{\Gamma}_{IJ_L} = \frac{5u_I + u_{J_L}}{6} \tag{10}$$

Inserting Equation (10) in Equation (9), we obtain

$$\nabla u_I = \frac{1}{V_I} \left[\sum_{L_I \in \Omega} \mathbf{C}_{IJ_L} \frac{(u_I + u_{J_L})}{2} + \sum_{L_I \in \Gamma} \mathbf{D}_{IJ_L} \frac{(5u_I + u_{J_L})}{6} \right] \tag{11}$$

It is worth emphasizing that the boundary term $(u^{\Gamma}_{IJ_L})$ defined in Equation (10) assumes a piecewise linear interpolation for boundary fluxes similar to a FEM type approximation, being formally second-order accurate in space when linear triangles are used [7]. The more traditional one-point flux approximation normally used in EBFV codes $(u^{\Gamma}_{IJ_L} = u_I)$ could also be used with some loss of accuracy along boundary nodes and their immediate neighbors [7, 15].

3.1. Non-isotropic and non-homogeneous media

In the case of heterogeneous media, fluxes definitions over the control surfaces located at the interface between different materials can be ambiguous [17]. If gradients computed as described in Equation (11) are directly used for flux computations, an inconsistent flux would be obtained

Copyright © 2008 John Wiley & Sons, Ltd.

DOI: 10.1002/fld

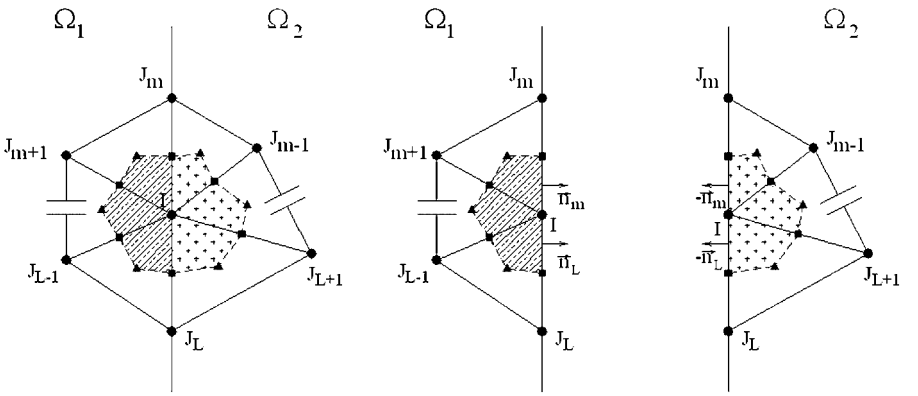

Figure 1. Two-dimensional control volume split by two different materials.

along the control surfaces adjacent to material discontinuities. In order to circumvent this problem, gradients are recovered in a sub-domain by sub-domain approach. First, material properties (e.g. permeability) are associated with sub-domains. For each physical sub-domain, we store a list of edges and nodes and their associated geometrical coefficients. For the mesh considered in Figure 1, it is necessary to include new geometrical coefficients $\mathbf{D}_{IJ_L} = A_L \mathbf{n}_L$ and $\mathbf{D}_{IJ_M} = A_M \mathbf{n}_M$, which are quantities related to the internal boundary edges in order to properly reconstruct gradients and fluxes in a particular sub-domain. These coefficients are used to properly recover the gradients for each physical sub-domain of the problem, allowing for a continuous by parts gradient computation. Therefore, for heterogeneous media, we can rewrite Equation (11) as

$$\nabla u_I^{\Omega_R} = \frac{1}{V_I^{\Omega_R}} \left[\sum_{L_{I(\Omega_R)}} \mathbf{C}_{IJ_L}^{\Omega_R} \frac{(u_I + u_{J_L})}{2} + \sum_{L_{I(\Gamma_{RE})}} \mathbf{D}_{IJ_L}^{\Omega_R} \frac{(5u_I + u_{J_L})}{6} + \sum_{L_{I(\Gamma_{RI})}} \mathbf{D}_{IJ_L}^{\Omega_R} \frac{(5u_I + u_{J_L})}{6} \right] \tag{12}$$

In Equation (12), $\nabla u_I^{\Omega_R}$ is the nodal gradient and $V_I^{\Omega_R}$ is the control volume of a node I associated with the sub-domain Ω_R, and $\mathbf{C}_{IJ_L}^{\Omega_R}$ and $\mathbf{D}_{IJ_L}^{\Omega_R}$ refer to the geometrical coefficients of the edge IJ_L associated with the sub-domain Ω_R. Finally, it is worth noting that in the present sub-domain by sub-domain approach, $\mathbf{D}_{IJ_L}^{\Omega_R}$ refers to both external and internal boundary edges, and Γ_{RE} and Γ_{RI} refer, respectively, to loops over external boundary edges and internal edges between multiple sub-domains. In order to compute the fluxes of Equation (5), we define a local frame of reference, in which one axis is placed along the edge direction (P), and another axis (N) is orthogonal to the direction (P), and split the gradients into two components

$$\nabla u_{IJ_L}^{\Omega_R} = \nabla u_{IJ_L}^{\Omega_R(N)} + \nabla u_{IJ_L}^{\Omega_R(P)} \tag{13}$$

The component of the gradient parallel to the edge direction $\nabla u_{IJ_L}^{\Omega_R(P)}$ is replaced by a local second-order central difference approximation $\nabla u_{IJ_L}^{\Omega_R(P^*)}$, see [10–12, 14, 15], and Equation (13) may be rewritten as

$$\nabla u_{IJ_L}^{\Omega_R^*} = \nabla u_{IJ_L}^{\Omega_R(N)} + \nabla u_{IJ_L}^{\Omega_R(P^*)} \tag{14}$$

Copyright © 2008 John Wiley & Sons, Ltd.

DOI: 10.1002/fld

where

$$\nabla u_{IJ_L}^{\Omega_R(P^*)} = \frac{(u_{J_L} - u_I)}{|\Delta_{IJ_L}|}\mathbf{L}_{IJ_L} \tag{15}$$

In Equation (15) $|\Delta_{IJ_L}|$ and $\mathbf{L}_{IJ_L} = \mathbf{IJ}_L/|\Delta_{IJ_L}|$ are, respectively, the length and the unity directional vector of the edge IJ_L. From Equation (13), the normal component of the gradient associated with the edge IJ_L can be computed as

$$\nabla u_{IJ_L}^{\Omega_R(N)} = \nabla u_{IJ_L}^{\Omega_R} - \nabla u_{IJ_L}^{\Omega_R(P)} \tag{16}$$

where the gradient along the edge direction is given by

$$\nabla u_{IJ_L}^{\Omega_R(P)} = (\nabla u_{IJ_L}^{\Omega_R} \cdot \mathbf{L}_{IJ_L})\mathbf{L}_{IJ_L} \tag{17}$$

with

$$\nabla u_{IJ_L}^{\Omega_R} = \frac{\nabla u_I^{\Omega_R} + \nabla u_{J_L}^{\Omega_R}}{2} \tag{18}$$

and the nodal gradients $\nabla u_I^{\Omega_R}$ and $\nabla u_{J_L}^{\Omega_R}$ are computed in a pure finite volume fashion as described in Equation (12).

Inserting Equation (17) in Equation (16) yields

$$\nabla u_{IJ_L}^{\Omega_R(N)} = \nabla u_{IJ_L}^{\Omega_R} - (\nabla u_{IJ_L}^{\Omega_R} \cdot \mathbf{L}_{IJ_L})\mathbf{L}_{IJ_L} \tag{19}$$

Inserting Equation (15) and Equation (19) in Equation (14), we have

$$\nabla u_{IJ_L}^{\Omega_R^*} = \nabla u_{IJ_L}^{\Omega_R} - (\nabla u_{IJ_L}^{\Omega_R} \cdot \mathbf{L}_{IJ_L})\mathbf{L}_{IJ_L} + \frac{(u_{J_L} - u_I)}{|\Delta_{IJ_L}|}\mathbf{L}_{IJ_L} \tag{20}$$

Defining the continuous 'hybrid' mid-edge flux function as

$$F_{IJ_L}^{\Omega_R^*} = -\underset{\sim}{K}^{\Omega_R} \nabla u_{IJ_L}^{\Omega_R^*} \tag{21}$$

in which the term hybrid was used to indicate that one part of the mid-edge gradient is computed using the traditional EBFV approach by averaging the nodal recovered gradients, and the other part is computed using the compact two-point finite difference scheme. Even though this hybrid approach may seem more complicated than both the usual TPFA and the simple nodal gradient averaging technique, it allows for the proper calculation of the cross diffusion terms, which is a major drawback of the TPFA, and, at the same time, it avoids the leap frog modes known as checkerboarding or odd–even oscillations that imply that the values computed at given node are uncoupled from the values of those nodes directly connected to it, which can occur when the simple nodal gradient averaging is used with orthogonal equally spaced quadrilateral meshes. In fact, it can be proved that these two usual techniques are inconsistent finite volume approximations for the discrete Laplacian operator on general triangular meshes [16].

It is worthy mentioning that EBFV schemes are linear preserving only in simplexes (triangular in two dimensional and tetrahedral in three dimensional) or orthogonal meshes (e.g. parallelepipeds). In a former paper [12] we have shown that the present method exactly recovers constant gradients when the solution varies linearly over the computational domain, i.e. it is linear preserving.

Copyright © 2008 John Wiley & Sons, Ltd.

DOI: 10.1002/fld

Linear preservation guarantees that a linear variation of a variable is integrated exactly on an arbitrary mesh. This property enforces that the order of the accuracy of the approximation is preserved, even for irregular, distorted or adapted meshes in which elements of different sizes and alignments are used all together. Therefore, extra care must be taken when dealing with non-orthogonal quadrilateral meshes. In the present paper, we have only used triangular and orthogonal quadrilateral meshes, and no study has been performed in order to evaluate the loss of accuracy associated with the use of non-orthogonal quadrilateral meshes.

Inserting Equation (20) in Equation (21), we can write

$$\mathbf{F}_{IJ_L}^{\Omega_R^*} = -\underset{\sim}{K}^{\Omega_R}\left(\nabla u_{IJ_L}^{\Omega_R} - (\nabla u_{IJ_L}^{\Omega_R}\cdot\mathbf{L}_{IJ_L})\mathbf{L}_{IJ_L} + \frac{(u_{J_L}-u_I)}{|\Delta_{IJ_L}|}\mathbf{L}_{IJ_L}\right) \tag{22}$$

Using the new surface flux approximation given by Equation (18) and Equation (22), we can redefine Equation (5) as

$$\sum_{R=1}^{N_{\text{dom}}}\left(\sum_{L_{I(\Omega_R)}}\mathbf{F}_{IJ_L}^{\Omega_R^*}\cdot\mathbf{C}_{IJ_L}^{\Omega_R} + \sum_{L_{I(\Gamma_R)}}\mathbf{F}_{IJ_L}^{\Gamma}\cdot\mathbf{D}_{IJ_L}^{\Omega_R}\right) = \sum_{R=1}^{N_{\text{dom}}} f_I^{\Omega_R} V_I^{\Omega_R} \tag{23}$$

and N_{dom} refers to the number of domains that surrounds node I, and the term $f_I^{\Omega_R}$ stands for the distributed source term associated with the volume $V_I^{\Omega_R}$ within the sub-domain Ω_R.

The expression above is built in a sub-domain by sub-domain basis (i.e. looping over sub-domains) in order to formally guarantee that the nodal gradients and fluxes are correctly approximated for each material along interface edges. It is worthy mentioning that the present approach is exact when the analytical solution for the scalar field u varies linearly, even for non-homogeneous materials, being far superior to formulations that use arithmetic or volume averaged procedures to associate permeabilities or other physical coefficients to edges [10, 12]. In the present EBFV formulation, even if the diffusion tensor is symmetric, the resulting system of equations, which has been solved using a simple sparse Gauss elimination solver, is in general, non-symmetric due to the inclusion of the cross diffusion terms. In some particular cases, for instance, when the media is isotropic and meshes are orthogonal, the resulting system of equations is symmetric.

4. ERROR EVALUATION

In order to evaluate the accuracy of the procedure used to compute the pressure field for problems with discontinuous and anisotropic coefficients, we define the asymptotic truncation error as [18]

$$\|E_h\| = Ch^q + O(h^{q+1}) \tag{24}$$

where h is the mesh spacing, q is the order of the error, which represents the convergence rate and C is a constant that is independent of h, and $\|\cdot\|$ is some specified norm. In this case, the convergence rate q is estimated as

$$q \cong \log_2 \frac{\|E_h\|}{\|E_{h/2}\|} \tag{25}$$

Copyright © 2008 John Wiley & Sons, Ltd.

DOI: 10.1002/fld

Following References [14, 18], the convergence rates were estimated using the following discrete norms: the maximum norm, $\|E\|_{\mathrm{MAX}}$, the L_2 norm, $\|E\|_{L_2}$ and the root mean square (RMS) norm, $\|E\|_{\mathrm{RMS}}$, which are respectively computed as

$$\|E\|_{\mathrm{MAX}} = \|\hat{u} - u\|_{L_{\mathrm{MAX}}} = \mathrm{MAX}\|\hat{u}_I - u_I\|, \quad I = 1, \ldots, NP \tag{26}$$

$$\|E\|_{L_2} = \|\hat{u} - u\|_{L_2} = \left(\sum_{I=1}^{NP} ((\hat{u}_I - u_I)^2 V_I) \right)^{1/2} \tag{27}$$

$$\|E\|_{\mathrm{RMS}} = \|\hat{u} - u\|_{L_{\mathrm{RMS}}} = \left(\sum_{I=1}^{NP} (\hat{u}_I - u_I)^2 \Big/ NP \right)^{1/2} \tag{28}$$

where u is the exact solution, $\hat{u}$ is the approximate solution and NP is the number of nodes of the computational mesh.

5. EXAMPLES

In this section we present the solutions obtained using the EBFV formulation described here for four benchmark problems found in literature and for which there are analytical and/or numerical solutions [14, 18–20]. In order to discretize the computational domain and evaluate the accuracy of the method, for the first three examples with smooth solutions, we have used a sequence of structured triangular or quadrilateral meshes with $NP = (9 \times 9)$, (17×17), (33×33) and (65×65), where N is the number of mesh nodes, and in which the triangular meshes were obtained by splitting quadrilaterals into two triangles, implying on triangular meshes with twice the number of elements but with the same number of nodes (i.e. CV). Numerical solutions were evaluated using the error norms and convergence rates defined in the previous section. For the fourth example, adapted from [20] to show the behavior of the method to solve a problem with high anisotropic non-smooth solution, we have used only an unstructured triangular mesh with $NP = (19 \times 19)$.

5.1. Homogeneous and isotropic media

This problem, which involves the solution of an elliptic equation in homogeneous and isotropic media, was presented in Reference [19], who solved it using two different methods: the traditional control volume finite element (CVFE) method, and the so-called control volume function approximation (CVFA) method, which is a locally conservative method in which different type of interpolation functions, such as splines, are used in the approximation process. In compact form, the problem can be described by the following equations:

$$\nabla(\underset{\sim}{K} \nabla u) = 2\pi^2 \cos(\pi x)\cos(\pi y) \quad \text{for } 0 < x < 1 \quad \text{and} \quad 0 < y < 1 \tag{29}$$

where the diffusion coefficient $\underset{\sim}{K}$ is defined by

$$\underset{\sim}{K} = \begin{pmatrix} 1 & 0 \\ 0 & 1 \end{pmatrix} \tag{30}$$

Copyright © 2008 John Wiley & Sons, Ltd.

DOI: 10.1002/fld

and boundary conditions are given by

$$\begin{aligned} \nabla u \cdot \underset{\sim}{n} &= 0 \quad \text{for } x=0,\ \ x=1 \text{ and } 0<y<1 \\ u &= \cos(\pi x) \quad \text{for } 0<x<1 \text{ and } y=0 \\ u &= -\cos(\pi x) \quad \text{for } 0<x<1 \text{ and } y=1 \end{aligned} \tag{31}$$

The periodic analytical solution for this problem is $u=\cos(\pi x)\cos(\pi y)$ defined throughout the unitary square domain $\Omega=(0,1)^2$. Figure 2 shows the scalar field u obtained using the (65×65) triangular mesh, which is in excellent agreement with the analytical solution.

In Tables I and II, we present the numerical errors and the convergence rates obtained in Reference [19], using the CVFE and the CVFA methods, respectively. In Table III, we present the errors and the convergence rates we have obtained using the EBFV method. As it can be seen, the three methods are second-order accurate for the scalar variable u, the results are similar, and our results compare slightly favorably to both the CVFE and the CVFA methods.

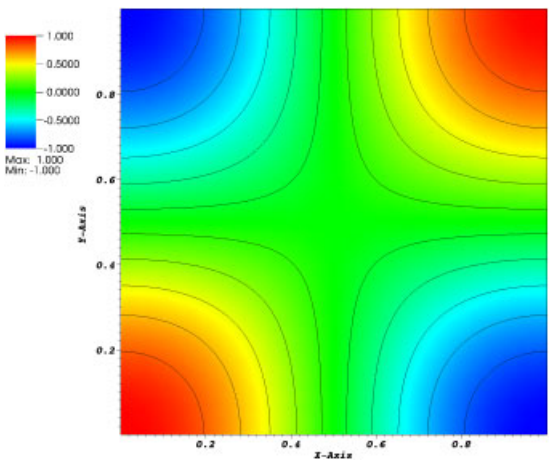

Figure 2. Elliptic equation with isotropic and continuous diffusion coefficient: scalar field u obtained with the EBFV using a (65×65) triangular mesh.

Table I. Numerical solution of the elliptic equation in homogeneous and isotropic media: errors and convergence rates for the CVFE [19].

N	$\|E\|_{L_2}$	q_{L_2}	$\|E\|_{\text{MAX}}$	q_{MAX}
8	1.57e−002	—	3.30e−002	—
16	4.00e−003	1.9757	8.77e−003	1.9138
32	1.00e−004	1.9939	2.25e−003	1.9625
64	2.51e−004	1.9985	5.69e−004	1.9827

Copyright © 2008 John Wiley & Sons, Ltd.

DOI: 10.1002/fld

Table II. Numerical solution of the elliptic equation in homogeneous and isotropic media: errors and convergence rates for the CVFA [19].

N	$\|E\|_{L_2}$	q_{L_2}	$\|E\|_{\mathrm{MAX}}$	q_{MAX}
8	1.21e−002	—	3.23e−002	—
16	3.00e−003	2.0199	8.35e−003	1.9531
32	7.45e−004	2.0087	2.10e−003	1.9875
64	1.85e−004	2.0050	5.27e−004	1.9968

Table III. Numerical solution of the elliptic equation in homogeneous and isotropic media: errors and convergence rates for the EBFV.

N	$\|E\|_{L_2}$	q_{L_2}	$\|E\|_{\mathrm{MAX}}$	q_{MAX}
8	5.18e−003	—	8.35e−003	—
16	1.23e−003	2.0738	2.13e−003	1.9727
32	3.01e−004	2.0327	5.35e−004	1.9936
64	7.50e−005	2.0147	1.34e−004	1.9985

5.2. Homogeneous and non-isotropic media

This problem was originally proposed by Crumpton in Reference [14], who solved it using cell-centered FCFV (Table IV). Hyman *et al.* [18] also solved this problem using the so-called mimetic finite differences formulations (MMFD) (Table V). Again, the considered domain is a unitary square, $\Omega=(0,1)^2$, with numeric Dirichlet boundary conditions extracted from the exact solution, which is given by $u=\mathrm{e}^{xy}$. In compact form, this problem can be described by

$$\nabla(\underset{\sim}{K}\nabla u)=-2(1+x^2+xy+y^2)\mathrm{e}^{xy} \tag{32}$$

where the diffusion tensor $\underset{\sim}{K}$ is given by

$$\underset{\sim}{K}=\begin{pmatrix}2 & 1\\ 1 & 2\end{pmatrix} \tag{33}$$

Figures 3(a) and (b) show, respectively, the initial triangular mesh with (9×9) nodes and the contours of the scalar field u for this mesh. As it can be seen in Table VI, the results obtained with our EBFV formulation are essentially second-order accurate in space. Besides, they are similar and compare favorably with those obtained in References [14, 18].

5.3. Non-homogeneous and non-isotropic media

The following example, which was originally presented in Reference [14], consists in a unity square, $\Omega=(0,1)^2$, formed by two different materials. In fact, numerical Dirichlet boundary conditions are obtained from the exact solution. Crumpton [14] solved this problem using a FCFV with structured orthogonal quadrilateral meshes. The problem can be compactly defined by

$$\nabla(\underset{\sim}{K}\nabla u)=f(x,y) \tag{34}$$

Copyright © 2008 John Wiley & Sons, Ltd.

DOI: 10.1002/fld

Table IV. Numerical solution of the elliptic equation in homogeneous and anisotropic media: errors and convergence rates for the FCFV [14].

N	$\|E\|_{\mathrm{RMS}}$	q_{RMS}
9	1.16e−003	—
17	2.89e−004	2.0050
33	7.28e−005	1.9891
65	1.83e−005	1.9921

Table V. Numerical solution of the elliptic equation in homogeneous and anisotropic media: errors and convergence rates for the MMFD [18].

N	$\|E\|_{L_2}$	q_{L_2}	$\|E\|_{\mathrm{MAX}}$	q_{MAX}
9	—	—	—	—
17	1.06e−003	—	3.74e−003	—
33	2.58e−004	2.0386	9.66e−004	1.9529
65	6.36e−005	2.0203	2.45e−004	1.9792

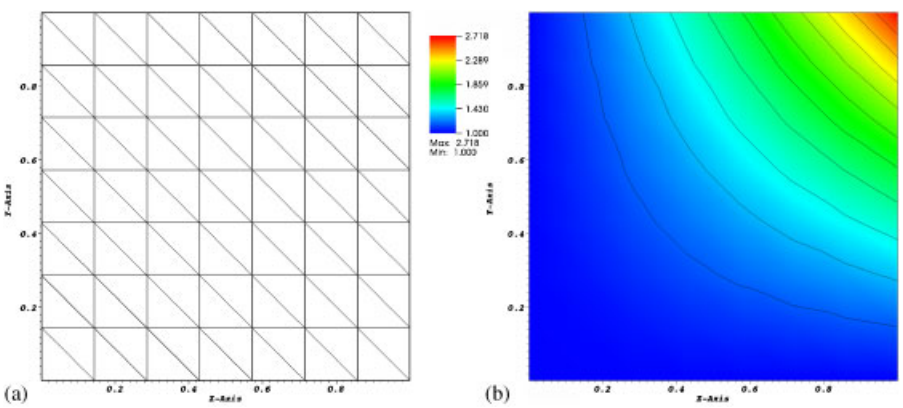

Figure 3. Homogeneous and anisotropic media: (a) triangular mesh (9×9) and (b) scalar field u.

Table VI. Numerical solution of the elliptic equation in homogeneous and anisotropic media: errors and convergence rates for the EBFV.

N	$\|E\|_{L_2}$	q_{L_2}	$\|E\|_{\mathrm{MAX}}$	q_{MAX}
9	—	—	—	—
17	1.06e−003	—	3.74e−003	—
33	2.58e−004	2.0386	9.66e−004	1.9529
65	6.36e−005	2.0203	2.45e−004	1.9792

Copyright © 2008 John Wiley & Sons, Ltd.

DOI: 10.1002/fld

where the discontinuous source term and the full tensor discontinuous diffusion coefficient are given, respectively, by

$$f(x,y)=\begin{cases}[-2\sin(y)-\cos(y)]\alpha x-\sin(y) & \text{for } x\leqslant 0\\ 2\alpha\exp(x)\cos(y) & \text{for } x>0\end{cases} \tag{35}$$

and

$$\underset{\sim}{K}=\begin{cases}\begin{pmatrix}1 & 0\\ 0 & 1\end{pmatrix} & \text{for } x<0\\ \alpha\begin{pmatrix}2 & 1\\ 1 & 2\end{pmatrix} & \text{for } x>0\end{cases} \tag{36}$$

where α controls the strength of the discontinuity (i.e. the jump in the material property) between the two different regions. The exact solution for this problem, given in Reference [14], is also presented in Equation (37).

$$u(x,y)=\begin{cases}[2\sin(y)+\cos(y)]\alpha x+\sin(y) & \text{for } x\leqslant 0\\ \exp(x)\cos(y) & \text{for } x>0\end{cases} \tag{37}$$

We have solved this problem using a sequence of uniform structured triangular and orthogonal quadrilateral meshes with $NP=(9\times 9)$, (17×17), (33×33) and (65×65) nodes. Figures 4(a)–(d) present the iso-contours of the scalar function $u(x,y)$ obtained by the EBFV method with the (65×65) triangular mesh associated with $\alpha=1.0$, $\alpha=10.0$, $\alpha=100.0$ and $\alpha=1000.0$, respectively.

Tables VII–X present the RMS errors, $\|E\|_{\mathrm{RMS}}$, and the convergence rates q_{RMS}, for the four different values of α obtained with the FCFV method of Crumpton [14] using orthogonal quadrilateral meshes, and the EBFV scheme using triangular and orthogonal quadrilateral meshes. As it can be clearly observed in Tables VII–X, for this particular benchmark problem, despite the fact that the increase of the strength of the discontinuity also increases the magnitude of the error for both methods, the EBFV and the FCFV methods show second-order spatial accuracy for all values of α. It can also be noted that for all tested cases, in terms of error norms, the EBFV scheme performs slightly worst (using triangular meshes) and slightly better (using quadrilateral meshes) than the FCFV method.

5.4. Homogeneous and non-isotropic problem with non-smooth solution

This last example was solved in Reference [20] using a cell-centered non-linear monotone finite volume (NLMFV) designed specifically to produce monotonic solutions (i.e. it preserves the positivity of the solution), in the presence of highly non-isotropic and heterogeneous materials. The computational domain consists in a unit square, with a square hole in the center $\Omega=(0,1)^2/[4/9,5/9]^2$ as shown in Figure 5. This problem can be briefly described as

$$\nabla(\underset{\sim}{K}\nabla u)=f(x,y) \tag{38}$$

where

$$\underset{\sim}{K}=\begin{pmatrix}\cos\theta & -\sin\theta\\ \sin\theta & \cos\theta\end{pmatrix}\begin{pmatrix}k_1 & 0\\ 0 & k_2\end{pmatrix}\begin{pmatrix}\cos\theta & \sin\theta\\ -\sin\theta & \cos\theta\end{pmatrix} \tag{39}$$

Copyright © 2008 John Wiley & Sons, Ltd.

DOI: 10.1002/fld

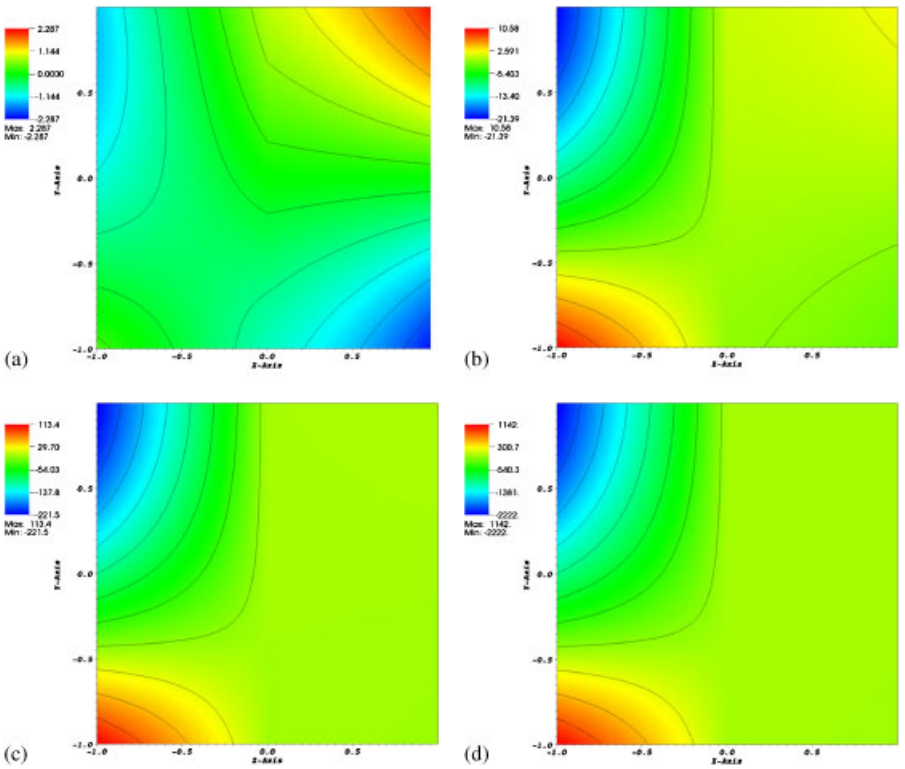

Figure 4. Iso-contours of the scalar function $u(x, y)$ obtained with the EBFV using a structured triangular mesh (65×65) for different values of α: (a) $\alpha = 1.0$; (b) $\alpha = 10.0$; (c) $\alpha = 100.0$; and (d) $\alpha = 1000.0$.

with $f(x, y) = 0$ and boundary conditions given by $u = 0$ on the external boundary, and $u = 2$ on the internal boundary, i.e.

$$\begin{aligned} u = 0 \quad \text{for} \quad & \begin{cases} 0 < x < 1 & \text{and} \quad (y = 0 \text{ or } y = 1) \\ 0 < y < 1 & \text{and} \quad (x = 0 \text{ or } x = 1) \end{cases} \\ u = 2 \quad \text{for} \quad & \begin{cases} \frac{4}{9} < x < \frac{5}{9} & \text{and} \quad (y = \frac{4}{9} \text{ or } y = \frac{5}{9}) \\ \frac{4}{9} < y < \frac{5}{9} & \text{and} \quad (y = \frac{4}{9} \text{ or } y = \frac{5}{9}) \end{cases} \end{aligned} \tag{40}$$

We have solved this problem using two different values for the angle $\theta = \pi/6$ and $\theta = 5\pi/6$. The ratio $k_1/k_2 = 1000$. There is no analytical solution for this problem, but results should clearly be bounded by boundary values throughout the domain (i.e. $0 \leqslant u(x, y) \leqslant 2$), with no 'overshoots' (i.e. $u(x, y) > 2$) or 'undershoots' (i.e. $u(x, y) < 0$). We have used an unstructured triangular mesh with an average mesh spacing of $h \approx \frac{1}{18}$. As it can be seen in Figure 6, our results are qualitatively similar to those obtained with the NLMFV of Reference [20]. Even though the EBFV generates no overshoots, it produces a reasonably amount of undershoots (almost 30% of non-Dirichlet nodes), whereas the NLMFV produces some overshoots. In fact, for the unstructured mesh used

Copyright © 2008 John Wiley & Sons, Ltd.

DOI: 10.1002/fld

Table VII. Numerical solution of the elliptic equation with anisotropic and discontinuous diffusion coefficient with $\alpha = 1.0$. Errors and convergence rates for the: (a) FCFV [14]; (b) EBFV—triangular meshes; and (c) EBFV—quadrilateral meshes.

N	$\|E\|_{\mathrm{RMS}}$	q_{RMS}
(a) FCFV—quad. meshes.		
9	3.33e−003	—
17	9.37e−004	1.8294
33	2.45e−004	1.9353
65	6.25e−005	1.9709
(b) EBFV—triang. meshes.		
9	6.02e−003	—
17	1.50e−003	1.9989
33	3.77e−004	2.0012
65	9.40e−005	2.0014
(c) EBFV—quad. meshes.		
9	3.19e−003	—
17	7.52e−004	2.0849
33	1.84e−004	2.0302
65	4.60e−005	1.9968

Table VIII. Numerical solution of the elliptic equation with anisotropic and discontinuous diffusion coefficient with $\alpha = 10.0$. Errors and convergence rates for the: (a) FCFV [14]; (b) EBFV—triangular meshes; and (c) EBFV—quadrilateral meshes.

N	$\|E\|_{\mathrm{RMS}}$	q_{RMS}
(a) FCFV—quad. meshes.		
9	1.62e−002	—
17	4.35e−003	1.9146
33	1.11e−003	1.9705
65	2.81e−004	1.9819
(b) EBFV—triang. meshes.		
9	4.57e−002	—
17	1.17e−002	1.9569
33	2.98e−003	1.9829
65	7.49e−004	1.9925
(c) EBFV—quad. meshes.		
9	4.27e−003	—
17	1.00e−003	2.0901
33	2.48e−004	2.0202
65	6.30e−005	1.9759

here, the minimum values for pressure were $u = -0.050$ for $\theta = \pi/6$, and $u = -0.052$ for $\theta = 5\pi/6$, respectively.

In order to improve the monotonicity of the solution, in Reference [20], authors suggest using a different strategy (inverse distance weighting) for interpolating the scalar variable u throughout

Copyright © 2008 John Wiley & Sons, Ltd.

DOI: 10.1002/fld

Table IX. Numerical solution of the elliptic equation with anisotropic and discontinuous diffusion coefficient with $\alpha = 100.0$. Errors and convergence rates for the: (a) FCFV [14]; (b) EBFV—triangular meshes; and (c) EBFV—quadrilateral meshes.

N	$\|E\|_{\mathrm{RMS}}$	q_{RMS}
(a) FCFV—quad. meshes.		
9	1.81e−001	—
17	4.74e−002	1.9330
33	1.21e−002	1.9699
65	3.04e−003	1.9929
(b) EBFV—triang. meshes.		
9	4.40e−001	—
17	1.13e−001	1.9538
33	2.88e−002	1.9813
65	7.24e−003	1.9916
(c) EBFV—quad. meshes.		
9	1.37e−002	—
17	3.26e−003	2.0699
33	7.96e−004	2.0364
65	1.97e−004	2.0149

Table X. Numerical solution of the elliptic equation with anisotropic and discontinuous diffusion coefficient with $\alpha = 1000.0$. Errors and convergence rates for the: (a) FCFV [14]; (b) EBFV—triangular meshes; and (c) EBFV—quadrilateral meshes.

N	$\|E\|_{\mathrm{RMS}}$	q_{RMS}
(a) FCFV—quad. meshes.		
9	1.83e−000	—
17	4.79e−001	1.9337
33	1.22e−001	1.9731
65	3.07e−002	1.9906
(b) EBFV—triang. meshes.		
9	4.39e−000	—
17	1.13e−000	1.9536
33	2.87e−001	1.9812
65	7.22e−002	1.9915
(c) EBFV—quad. meshes.		
9	1.46e−001	—
17	3.50e−002	2.0635
33	8.51e−003	2.0391
65	2.09e−003	2.0210

the domain, instead of using the more traditional linear interpolation technique. Besides, they have also established that no overshoots are observed with the NLMFV when the sharp gradients of the solution are aligned with the mesh edges. This example clearly shows that further improvements

Copyright © 2008 John Wiley & Sons, Ltd.

DOI: 10.1002/fld

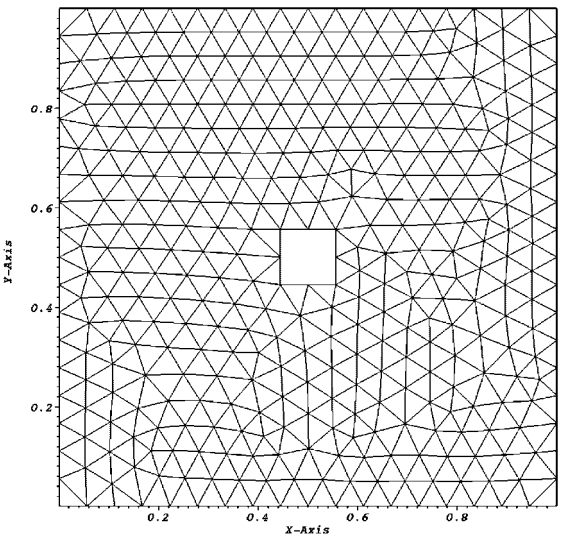

Figure 5. Geometry and unstructured triangular mesh used to solve the homogeneous and non-isotropic problem with non-smooth solution.

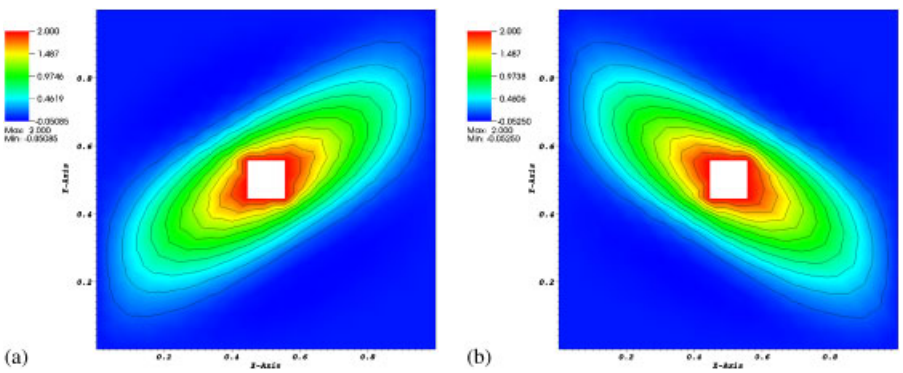

Figure 6. Numerical solution for the homogeneous and non-isotropic problem with non-smooth solution: (a) rotation angle $\theta=\pi/6$ and (b) rotation angle $\theta=5\pi/6$.

must be made to the EBFV if ones must guarantee monotone results for really challenging problems.

6. CONCLUSIONS

In the present paper we have presented some results on the accuracy of an edge-based node-centered finite volume formulation (EBFV), which can be used to solve elliptic type equations with highly discontinuous coefficients. These elliptic equations are quite common in heat conduction

Copyright © 2008 John Wiley & Sons, Ltd.

DOI: 10.1002/fld

problems and flux flow through porous media, such as the two-phase flow of oil and water in petroleum reservoirs and the transport of contaminants in aquifers. Full tensors (non-diagonal diffusion coefficients) and flexible (unstructured) non-orthogonal meshes are naturally handled by the EBFV formulation and the cross diffusion terms are properly computed. In order to show the potential of the presented finite volume procedure, we have solved four benchmark problems that involve diagonal and continuous, non-diagonal and continuous and non-diagonal and discontinuous diffusion coefficients, as well as continuous and discontinuous distributed source terms, and a problem with a highly non-smooth solution. In the first three cases, second-order accuracy for the scalar variable (e.g. pressure) has been achieved using different discrete norms. The last example has show that, in the case of non-smooth solutions, the EBFV does not formally guarantee monotonocity and, certainly, further improvements can be made to the method. In the near future we intend to study possible fixes for the lack of monotonicity of the method when dealing with really challenging problems. Despite of the later remark, our results (not fully presented here) are quite promising and compare favorably with other results found in literature.

ACKNOWLEDGEMENTS

The authors would like thank the following Brazilian research agencies: Conselho Nacional de Desenvolvimento Científico e Tecnológico (CNPq), Agência Nacional do Petróleo (ANP-MCT), Fundação de Amparo à Ciência e Tecnologia do Estado de Pernambuco (FACEPE).

REFERENCES

1. Edwards MG, Rogers CF. Finite volume discretization with imposed flux continuity for the general tensor pressure equation. *Computational Geosciences* 1998; **2**:259–290.
2. Ewing RE. *The Mathematics of Reservoir Simulation*. SIAM: Philadelphia, 1983.
3. Aavatsmark I, Barkve T, Bøe Ø, Mannseth T. Discretization on unstructured grids for inhomogeneous, anisotropic media. Part I: derivation of the methods. *SIAM Journal on Scientific Computing* 1998; **19**:1700–1716.
4. Edwards MG. M-matrix flux splitting for general full tensor discretization operators on structured and unstructured grids. *Journal of Computational Physics* 2000; **160**:1–28.
5. Klausen RA, Eigestad GT. Multi-point flux approximations and finite element methods: practical aspects of discontinuous media. *9th European Conference on the Mathematics of Oil Recovery*, Cannes, France, 2004.
6. Loula AFD, Garcia ELM, Coutinho ALGA. Miscible displacement simulation by finite element methods in distributed memory machines. *Computer Methods in Applied Mechanics* 1999; **174**:339–354.
7. Luo H, Baum JD, Löhner R. An improved finite volume scheme for compressible flows on unstructured grids. *Technical Report*, 1995. AIAA Paper 95-0348.
8. Crumpton PI, Moinier P, Giles MBTJ. An unstructured algorithm for high Reynolds number flows on highly stretched grids. In *Numerical Methods in Laminar and Turbulent Flow*, Taylor C, Cross JT (eds). Pineridge Press: Swansea, 1997; 561–572.
9. Lyra PRM, Lima RCF, Guimarães CSC, Carvalho DKE. An edge-based unstructured finite volume procedure for the numerical analysis of heat conduction applications. *Journal of the Brazilian Society of Mechanical Science and Engineering* 2004; **26**:160–169.
10. Rees I, Masters I, Malan AG, Lewis RW. An edge-based finite volume scheme for saturated–unsaturated groundwater flow. *Computer Methods in Applied Mechanics* 2004; **193**:4741–4759.
11. Carvalho DKE, Lyra PRM, Willmersdorf RB, Araújo FDS. An unstructured edge-based finite volume formulation for solving immiscible two-phase flows in porous media. *Communications in Numerical Methods in Engineering* 2005; **21**:747–756.
12. Carvalho DKE, Willmersdorf RB, Lyra PRM. A node-centered finite volume formulation for the solution of two-phase flows in non-homogeneous porous media. *International Journal for Numerical Methods in Fluids* 2007; **53**:1197–1219.

Copyright © 2008 John Wiley & Sons, Ltd.

DOI: 10.1002/fld

13. Lyra PRM, Morgan K. A review and comparative study of upwind biased schemes for compressible flow computations: Part III: multidimensional extension on unstructured grids. *Archives of Computational Methods in Engineering* 2002; **9**(7):207–256.
14. Crumpton PI. Discretization and multigrid solution of elliptic equations with mixed derivative terms and strongly discontinuous coefficients. *Journal of Computational Physics* 1995; **116**:343–358.
15. Sorensen KA. A multigrid accelerated procedure for the solution of compressible fluid flows on unstructured meshes. *Ph.D. Thesis C/Ph/161/01*, Department of Civil Engineering, University of Wales/Swansea, U.K., 2001.
16. Svärd M, Nordström J. A stable and accurate summation by parts finite volume formulation of the Laplacian operator. *Technical Report 003*, Institutionen för Informationsteknologi, Uppsala Universitet, 2003; 1–36.
17. Helmig R, Huber R. Comparison of Galerkin-type discretization techniques for two-phase flow problems in heterogeneous porous media. *Advances in Water Resources* 1998; **21**:697–711.
18. Hyman J, Shashkov M, Steinberg S. The numerical solution of diffusion problems in heterogeneous non-isotropic materials. *Journal of Computational Physics* 1997; **132**:130–148.
19. Chen Z, Huan G, Ma Y. *Computational Methods for Multiphase Flows in Porous Media*. SIAM: Philadelphia, 2006.
20. Lipnikov K, Shaskov M, Svyatskiy D, Vassilevski Yu. Monotone finite volume schemes for diffusion equations on unstructured triangular and shape-regular polygonal meshes. *Journal of Computational Physics* 2007; **227**: 492–512.

Copyright © 2008 John Wiley & Sons, Ltd.

DOI: 10.1002/fld